

# A physical approach to modify the hydraulic reactivity of $\alpha$ -tricalcium phosphate powder

Marc Bohner<sup>a,\*</sup>, Reto Luginbühl<sup>a</sup>, Christian Reber<sup>b</sup>, Nicola Doebelin<sup>a</sup>,  
Gamal Baroud<sup>c</sup>, Egle Conforto<sup>d</sup>

<sup>a</sup> RMS Foundation, Bismattstrasse 12, P.O. Box 203, CH-2544 Bettlach, Switzerland

<sup>b</sup> Département de Chimie, Université de Montréal, Montréal, Que., Canada H3C 3J7

<sup>c</sup> Laboratoire de Biomécanique, Département de Génie, Université de Sherbrooke, Sherbrooke, Que., Canada J1K 2R1

<sup>d</sup> Fédération de Recherche en Environnement pour le Développement Durable (FR-EDD), FR CNRS 3097, Centre Commun d'Analyses, 5 Allées de l'Océan, F-17071 La Rochelle Cedex 9, France

Received 21 January 2009; received in revised form 18 May 2009; accepted 19 May 2009

Available online 24 May 2009

## Abstract

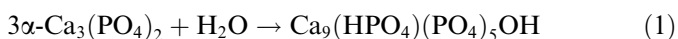
A microsized  $\alpha$ -tricalcium phosphate ( $\alpha$ -TCP) powder was calcined at various temperatures ( $350\text{ }^{\circ}\text{C} < T < 800\text{ }^{\circ}\text{C}$ ) for various durations (1–24 h) and the resulting physico-chemical and reactivity changes were measured. Without calcination, the  $\alpha$ -TCP powder started reacting within minutes after contacting a 0.2 M  $\text{Na}_2\text{HPO}_4$  solution as measured by isothermal calorimetry. The overall reaction was finished within a few days. After calcination at  $350\text{ }^{\circ}\text{C} \leq T \leq 550\text{ }^{\circ}\text{C}$  for 24 h, no significant changes in the crystalline composition, crystallite size, particle size or specific surface area were noticed. However, the powder reactivity was progressively changed. More specifically, the hydraulic reaction of the powders calcined at 500 and 550  $^{\circ}\text{C}$  only started after 2–3 h whereas the overall hydraulic reaction was only slightly postponed, suggesting that physical or chemical changes had occurred at the particle surface. As mainly physical changes were detected at the particle surface during calcination at 500  $^{\circ}\text{C}$ , it was speculated that the appearance of this reaction delay (= induction time) was due to the disappearance of surface defects during the calcination step, i.e. to the need to create surface defects to induce dissolution and hence reaction.

© 2009 Acta Materialia Inc. Published by Elsevier Ltd. All rights reserved.

**Keywords:**  $\alpha$ -Tricalcium phosphate; Biomaterials; Hydroxyapatite; Isothermal calorimetry; Calcium phosphate cement

## 1. Introduction

Calcium phosphate cements (CPCs) have been used as bone substitute for the last two decades [1]. Generally, they consist of a mixture of an aqueous solution and one or several calcium phosphate powders [2]. Many CPC formulations have been proposed, in particular those based on the use of  $\alpha$ -tricalcium phosphate ( $\alpha$ -TCP;  $\text{Ca}_3(\text{PO}_4)_2$ ) [3]. The idealized setting reaction of  $\alpha$ -TCP-based CPCs is [4,5]:



$\alpha$ -TCP powders used in CPCs are generally obtained by a combination of sintering and milling procedures [4–6], present a mean particle size of 1–10  $\mu\text{m}$  [7–9] and start reacting within seconds after contacting an aqueous solution [7,10].

To be used clinically, CPCs need to have appropriate handling properties, in particular an adapted setting rate [11]. Ideally the cement should hardly react during mixing and application, and then rapidly harden. To achieve this, additives such as phosphate ions or hydroxyapatite (HA) seed crystals have been added to  $\alpha$ -TCP-based CPC formulations [8,12]. Another approach is to prolong the milling duration of the raw materials to make them more reactive [7,13,14]. Unfortunately, these approaches are not good

\* Corresponding author. Tel.: +41 326441413; fax: +41 326441176.

E-mail address: [marc.bohner@rms-foundation.ch](mailto:marc.bohner@rms-foundation.ch) (M. Bohner).

enough for applications such as vertebroplasty (reinforcement of vertebral bodies with cement), for which the viscosity during application should be in a defined range, and hardening should then proceed fast [15]. Thus, there is a need to find new and better ways to control and increase the CPC setting rate.

Recently, it was found that nanosized  $\alpha$ -TCP powders obtained by calcining (= thermally treating = tempering) amorphous TCP powders at 600–700 °C reacted quickly but only after an induction period of several hours [16,17]. This long induction time was attributed to the difficulty in creating surface defects, which are essential for the initiation of particle dissolution [18]. It was speculated that the absence of surface defects in these nanosized  $\alpha$ -TCP powders was due to the application of a thermal treatment. Therefore, the aim of this study was to elucidate the influence of calcination on the hydraulic reactivity of microsized  $\alpha$ -TCP powders obtained by sintering and milling.

## 2. Materials and methods

### 2.1. Raw materials

A 2:1 M ratio blend of calcium carbonate powder (CC,  $\text{CaCO}_3$ ; Merck, Germany, Art No. 102076) and dicalcium phosphate powder (DCP,  $\text{CaHPO}_4$ ; GFS Chemical, USA, Art No. 1548) was mixed end-over-end for 1 h using a Turbula mixer (Bachofen, Switzerland). It was then calcined at 900 °C for 1 h in an LHT 02/16 furnace (Nabertherm, Germany), cooled to room temperature and ground in a mortar with a pestle until all could pass through a 0.125 mm sieve. The calcined and sieved blend was then placed on calcium-stabilized  $\text{ZrO}_2$  plates (S-3406, Zircoa, USA), sintered at 1350 °C for 4 h and then removed from the furnace to quench the powder in air. The sintered powder was then broken in a jaw crusher (BB51, Retsch, Germany) to the point at which all material could pass through a 0.125 mm sieve. Finally, the powder was ball milled in a planetary mill (Pulverisette 5, Fritsch, Germany). The selected conditions were: 100 g of powder with 0.5 ml of ethanol and 100  $\text{ZrO}_2$  spheres (weighing 3 g each), milled at 400 rpm for 15 min ( $\text{ZrO}_2$  containers). The resulting powder was dried at 60 °C until constant weight was reached and rapidly homogenized by hand (100 end-over-end moves). This powder was used as the starting material for all other powders. Below, it is referred to as “powder 1”.

### 2.2. Tested parameters

Several parameters were investigated: the influence of the duration and the temperature of the calcination step, as well as the effect of milling calcined powders (3 min in the planetary mill using the same conditions described herein) on the hydraulic reactivity of powder–liquid mixtures (Table 1). It is worth mentioning that the “starting” or “untreated” powder (powder 1) used here to produce

all other powders can be considered to be a thermally treated powder at room temperature (20–25 °C) for a duration of several months (duration of all experiments).

### 2.3. Characterizations

The powders were characterized by several means: (i) laser scattering to determine the particle size distribution (PSD), (ii) nitrogen adsorption to determine the specific surface area (SSA) using the BET model; (iii) scanning electron microscopy (SEM) to assess the morphology of the powders; (iv) X-ray diffraction (XRD) to assess the crystalline composition; (v) X-ray photoelectron spectroscopy (XPS); (vi) micro-Raman spectroscopy to identify chemical changes at the particle surfaces; (vii) isothermal calorimetry to assess the powder reactivity; and (viii) finally transmission electron microscopy (TEM) to observe the presence and spatial distribution of crystalline and amorphous phases.

The PSD was measured by laser scattering (Mastersizer 2000, Malvern, USA). For this purpose, the  $\alpha$ -TCP powder was dispersed in ethanol and a model assuming Mie scattering with a particle refractive index and absorption of 1.60 and 0, respectively, was used for data inversion. The modeling parameters, as well as other instrument settings like pump speed and ultrasound level, were tested and showed no influence on the results. At least three measurements were made per powder.

The SSA was measured by nitrogen adsorption using a BET model (Gemini 2360, Micromeritics, USA). Four measurements were made per powder.

For SEM, particles were placed on a sticky carbon tape, itself glued onto an aluminium sample holder. The particles were then sputtered with C and subsequently with Au to a total thickness of approximately 20 nm. The samples were observed with a Cambridge S360 microscope (Leica, Germany) and an EVO MA25 microscope (Zeiss, Germany).

For XRD the powder was homogenized and packed in a cavity in an aluminium sample holder. XRD data were collected in reflective geometry on a Philips PW1800 diffractometer (Philips, Eindhoven, The Netherlands) equipped with a graphite monochromator in the secondary beam.  $\text{Cu K}_\alpha$  radiation and a step size of 0.02° were used to measure  $2\theta$  from 4.01 to 59.99°. Rietveld refinements for quantitative phase analysis were done with the computer program FullProf.2k (Version 3.40) [19] using a previously determined instrument resolution function. Starting models for the quantified phases were taken from Schroeder et al. [20] for  $\beta$ -TCP (whitlockite model, but with fully Ca-occupied sites), Mathew et al. [21] for  $\alpha$ -TCP and Sudarsanan et al. [22] for HA. Average crystallite sizes were calculated from isotropic peak broadening using the Scherrer equation.

XPS measurements were performed on a Kratos Axis Nova spectrometer (Kratos Analytical, Manchester, UK) equipped with a monochromatic  $\text{Al K}_\alpha$  source (1486.7 eV, 225 W). Charge-neutralized survey spectra

Table 1  
List of parameters investigated in this study and their levels.

Investigated parameters	Parameter levels
Series 1: Calcination temperature	350, 400, 450, 500, 550, 600 and 700 °C
Series 2: Calcination duration	0, 1, 5 and 24 h
Series 3: Calcination/milling cycles	Powder 1: no treatment (= “raw” powder) Powder 2: C Powder 4: C × M Powder 6: C × M × C Powder 9: C × M × C × M

C, calcination at 500 °C for 1 h; M, milling in the planetary mill for 3 min at 400 rpm; C × M × C, calcination + milling + calcination step.

were acquired in slot mode (0.3 cm<sup>2</sup> illuminated area) at a pass energy of 80 eV between 1450 and −5 eV with a step size of 0.5 eV, while detailed spectra were acquired at single elements with a pass energy of 40 eV and a step size of 0.1 eV. All spectra were adjusted and referenced to the binding energy of the aliphatic carbon C–H component at 285 eV. The spectra were analysed using CasaXPS software (V2.3.14, Casa Software Ltd., UK). Quantification was obtained after subtraction of an iterated Shirley background and by applying corrected sensitivity factors given by Kratos.<sup>1</sup> The powder samples were mounted on a custom-built Teflon powder holder with sample wells of 5 mm diameter. Several spectra were acquired for each sample. Commercial ultrapure HA (No. 574791, Aldrich; purity: 99.999%) and calcium carbonate (No. 202932, Aldrich; purity: 99.995%) served as the reference and control, respectively.

Micro-Raman spectra were measured with a Renishaw Invia system equipped with a Leica microscope. Spectra were measured on samples as obtained without any further treatment. A diode laser with a wavelength of 782 nm was used as the excitation source. This near-infrared excitation led to better quality spectra than visible excitation from an argon ion laser.

An eight-station isothermal calorimeter (TAM Air Cement, Thermometric AB, Sweden) was used to study the reaction kinetics after mixing a calcium phosphate powder mixture with 1 ml of aqueous solution. Experiments were performed with 2.0 g of  $\alpha$ -TCP powder and 1.0 ml of 0.2 M sodium phosphate solution. The pH of the solution was varied according to Table 1. The powder was put in the sealed compartment of the mixing cell (the “20 ml admix ampoule”) while the liquid was put into the injection compartment of the cell. Subsequently, the loaded cell was lowered into the calorimeter and kept at a temperature of 37 °C until equilibrium was reached. When a constant (zero) signal was reached, the solution was injected into the powder and mixed with it using the mixing rod. The measurements were

terminated when a constant thermal signal had been reached (typically after 1–7 days). At least four randomized measurements were made per powder. To assess the powder reactivity, it was assumed that the degree of reaction was proportional to the fraction of released heat (more details can be found elsewhere [10]). As a result, the evolution of the cumulated released heat was considered to be representative of the evolution of the degree of reaction. Three points along the “released heat fraction =  $f(\text{time})$ ” curve were selected, i.e. at 10%, 50% and 90% released heat (100% was assumed to correspond to the total amount of heat released at the end of the setting reaction) to assess the influence of the chemistry on the kinetics of the cement setting reaction. These points were selected because CPC setting time corresponds typically to a reacted fraction close to 10% while the mechanical properties reach a plateau close to a reacted fraction of 90% [12,23]. The 50% point was selected as an intermediate value between 10% and 90%. Furthermore, the total released heat was determined (expressed in J g<sup>−1</sup>) when the signal had reached its baseline, typically after 3–4 days. The sodium phosphate mixing solution (0.2 M) was chosen since the mixing liquid of most  $\alpha$ -TCP-based CPC formulations contains phosphate ions. The control experiment with pure water did not result in significant differences (data not reported here).

The transmission electron microscope used was a JEOL JEM-2011, operated at 200 kV, with a resolution of 0.25 nm. It was equipped with an Oxford Link ISIS EDS system and a Gatan Dualview CDD camera. Images were obtained in bright and dark field modes. A double-tilt specimen holder was used to spatially orient crystals in selected area electron diffraction mode. This procedure allowed the identification of crystalline phases through the indexation of mono- and polycrystal diffractograms. Low-concentration dispersions of calcium phosphate particles in ultrapure ethanol were submitted to ultrasound agitation for 15 min. The goal was to separate particles forming agglomerates and to obtain homogeneous dispersions. These were then dropped on transmission electron microscope grids covered with carbon films. After ethanol evaporation, observable calcium phosphate particles lay upon the surface of the film.

### 3. Results

According to XRD, all the  $\alpha$ -TCP powders used in this study had a purity close to 95%, and contained a few percent of  $\beta$ -TCP and HA (Fig. 1 and Table 2). Submitting the powder to calcination–milling cycles or to calcination durations of up to 24 h at 500 °C had no significant effect on the powder phase composition (Table 2). Crystalline phase changes were only observed at and above a temperature of 600 °C (Fig. 1 and Table 2).

The crystallite size of  $\alpha$ -TCP powders was close to 50–60 nm up to 550 °C (Table 2). The size increased to about 100 nm at 600–700 °C. A change in the calcination duration at 500 °C did not change the  $\alpha$ -TCP crystallite size significantly, though the size did tend to decrease (Table 2).

<sup>1</sup> Note: there is no original literature. The sensitivity factors are factory/instrument-based factors which were verified and, if necessary, corrected by us in extensive calibration procedures for the most important elements.

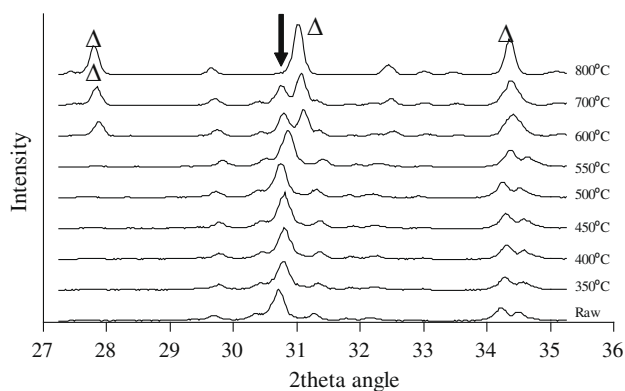


Fig. 1. XRD spectra of  $\alpha$ -TCP powder calcined for 24 h at various temperatures. A shift of 600 counts  $s^{-1}$  was added between each curve. The position of the main diffraction peaks of  $\beta$ -TCP are indicated by a  $\Delta$ . The position of the main  $\alpha$ -TCP diffraction peak is shown with an arrow.

Powders submitted to calcination–milling cycles presented a continuous decrease in crystallite size (Table 2). Importantly, all these effects were not statistically significant, because only one XRD measurement was made for each condition, but they provide some information on the effect of calcination and milling.

The particle size distribution expressed in volume frequency was bimodal, with maxima at 5–6 and 50–60  $\mu\text{m}$  and a mean diameter ( $d_{(50)}$  in volume) close to 10  $\mu\text{m}$  (Fig. 2a). In contrast, the particle size distribution was monomodal, with a mean diameter close to 1.8  $\mu\text{m}$  when

expressed in number frequency. No significant change was noticed with various calcination–milling cycles (Fig. 2b). Even the powders calcined at 800  $^{\circ}\text{C}$  for 1 h presented no significant change in mean particle size ( $d_{(50)} = 9.7$ ; standard deviation = 0.1  $\mu\text{m}$ ).

Significant changes in the SSA values were observed to occur subsequently to calcination but only at and above 600  $^{\circ}\text{C}$  (Table 2): the SSA values were reduced from about 2.2–2.3 to 1.0  $\text{m}^2 \text{g}^{-1}$  after 24 h at 800  $^{\circ}\text{C}$ . The SSA values of calcined and milled samples suggest that a 1 h calcination at 500  $^{\circ}\text{C}$  reduced the SSA values slightly whereas milling the powders for 3 min increased them slightly (Table 2). The SSA values appeared to increase with each calcination–milling cycle (from 2.2–2.3 to 2.7–2.8  $\text{m}^2 \text{g}^{-1}$ ; Table 2).

The general morphology of the raw powder is revealed by SEM (Fig. 3). The powder consisted of rough micro-sized particles. Calcining the powder at 500  $^{\circ}\text{C}$  for 24 h did not modify the general aspect of the particles. However, there was a (non-significant) trend towards a decrease in the particle nanoroughness, as pointed out with the arrows in Fig. 3. This effect is seen more clearly when looking at large  $\alpha$ -TCP particles (particles only milled in the jaw crusher and not subsequently in the planetary mill; size: 0.125–0.180 mm) calcined at 500  $^{\circ}\text{C}$  for 24 h: nanosized defects present on the surface of the crushed particles disappeared during calcination (Fig. 4). On the latter photos, it can be seen that some of the surface roughness is due to the presence of loose particles on the surface (see arrows).

Table 2

Effect of temperature and calcination duration on the physical properties of  $\alpha$ -TCP powders: XRD composition (Rietveld refinement), XRD crystallite size (Rietveld refinement), mean particle size in volume (PSD data) and specific surface area (applying the BET model on  $\text{N}_2$  adsorption results or inferred from PSD measurements).

Denomination	Thermal treatment		Refined XRD composition (%)			Crystallite size (nm) ( $\alpha$ -TCP)	Mean particle size in volume ( $\mu\text{m}$ )			Specific surface area ( $\text{m}^2 \text{g}^{-1}$ )	
	Temperature ( $^{\circ}\text{C}$ )	Duration (h)	$\alpha$ -TCP	$\beta$ -TCP	HA		$d_{(10)}$	$d_{(50)}$	$d_{(90)}$	$\text{N}_2$ adsorption	From PSD
Powder 1	–	–	94.9	2.5	2.6	58	2.7 (0.1) <sup>a</sup>	9.4 (1.0)	87 (27)	2.3 (0.0)	1.0 (0.0)
Powder 2 (C) <sup>b</sup>	500	1	94.6	2.5	3	57	2.8 (0.0)	8.7 (0.2)	75 (0)	2.2 (0.1)	1.0 (0.0)
Powder 2.10	500	5	94	2.7	3.3	54	n.m. <sup>d</sup>	n.m.	n.m.	2.3 (0.1)	n.m.
Powder 2.1	500	24	92.7	3.3	4	54	n.m.	n.m.	n.m.	2.6 (0.1)	n.m.
Powder 2.3	350	24	94.3	2.4	3.3	51	n.m.	n.m.	n.m.	2.3 (0.1)	n.m.
Powder 2.4	400	24	94.1	2.7	3.2	55	n.m.	n.m.	n.m.	2.2 (0.1)	n.m.
Powder 2.5	450	24	94.4	2.9	2.8	54	n.m.	n.m.	n.m.	n.m.	n.m.
Powder 2.6	550	24	94.3	2.6	3.2	55	n.m.	n.m.	n.m.	2.3 (0.0)	n.m.
Powder 2.7	600	24	46.8	51.2	1.9	102	n.m.	n.m.	n.m.	1.3 (0.1)	n.m.
Powder 2.8	700	24	37.2	60.4	2.4	103	n.m.	n.m.	n.m.	1.3 (0.1)	n.m.
Powder 2.9	800	24	0.1	99.6	0.3	–	n.m.	n.m.	n.m.	1.0 (0.1)	n.m.
Powder 4 (C $\times$ M) <sup>c</sup>	500	1	94.8	2.3	2.9	53	2.3 (0.0)	9.4 (1.0)	77 (9)	2.7 (0.1)	1.1 (0.1)
Powder 6 (C $\times$ M $\times$ C)	500	1	94.1	2.5	3.4	48	2.5 (0.0)	10.3 (0.3)	84 (7)	2.5 (0.0)	1.0 (0.0)
Powder 9 (C $\times$ M $\times$ C $\times$ M)	500	1	94.3	2.4	3.4	43	2.2 (0.1)	8.6 (1.4)	55 (11)	2.8 (0.1)	1.2 (0.1)
Powder 3	800	1	28	70.8	1.2	133	3.5 (0.0)	9.7 (0.1)	74 (0)	1.2 (0.0)	0.8 (0.0)

See Table 1 for additional details regarding the denomination of the powders.

<sup>a</sup> Figures in parentheses are standard deviations.

<sup>b</sup> C, calcination (1 h @ 500  $^{\circ}\text{C}$ ).

<sup>c</sup> M, milling at 400 rpm for 3 min; C  $\times$  M, calcination + milling.

<sup>d</sup> n.m., not measured.

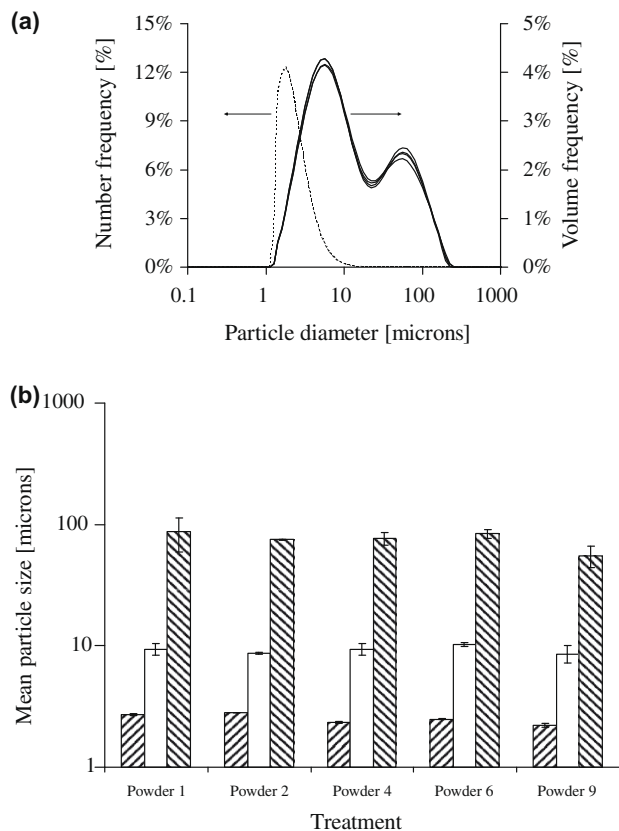


Fig. 2. (a) Particle size distribution in number and volume of powder 1 (four measurements are shown) and (b) mean particle size as a function of powder treatment. Three histogram bars are shown per powder. These bars correspond to the following values:  $d_{(10)}$ ,  $d_{(50)}$  and  $d_{(90)}$ . Treatment denomination: C, calcination at 500 °C for 1 h; M, milling in the planetary mill for 3 min at 400 rpm. The results of powder 1 (here shown by “—”), powder 2 (“C”), powder 4 (“C × M”), powder 6 (C × M × C, calcination + milling + calcination step) and powder 9 (C × M × C × M) are shown.

TEM observations revealed the presence of  $\alpha$ -TCP and HA particles in both powder 1 (untreated powder) and powder 2.1 (calcined at 500 °C for 24 h). An amorphous phase was detected in powder 1 (Fig. 5), whereas  $\beta$ -TCP particles were identified in powder 2.1. In general, powder 2.1 appeared more crystalline than powder 1. However, since only about 20 of the thinnest particles were looked at in both powder 1 and powder 2.1, these observations are qualitative rather than quantitative.

Calcining  $\alpha$ -TCP powder had a strong effect on its reaction rate as measured by calorimetry (Figs. 6 and 7): the main reaction peak of powders calcined at or above 500 °C (powder 2.1 and powders 2.3–2.9) was delayed from a few minutes to several hours during the reaction (Fig. 6). In parallel, a 15% decrease in the cumulated heat release was measured while increasing the calcination temperature up to 550 °C (Fig. 7). Calcining  $\alpha$ -TCP powder at 600 (powder 2.7) and 700 °C (powder 2.8) extended the induction period even more and markedly reduced the cumulated heat release due to a partial conversion of  $\alpha$ -TCP into  $\beta$ -TCP (Fig. 7).

A change in reactivity was observed in  $\alpha$ -TCP powder calcined for 1 h at 500 °C (powder 2; Figs. 8 and 9), even though a more pronounced effect was measured for calcination durations of 5 and 24 h (powders 2.10 and 2.1). Interestingly, no significant change in cumulated released heat was observed between 1 and 24 h calcination (Fig. 9).

The milling of  $\alpha$ -TCP powder for 3 min after calcination eliminated the induction period observed during the hydraulic reaction of calcined powders (Fig. 10). In fact, the results obtained with various calcination–milling cycles suggest that this passivation effect of calcination is reversible provided mechanical energy is applied on the powder.

Interestingly, the colour of the calcined  $\alpha$ -TCP powders changed depending on the calcination temperature. It was

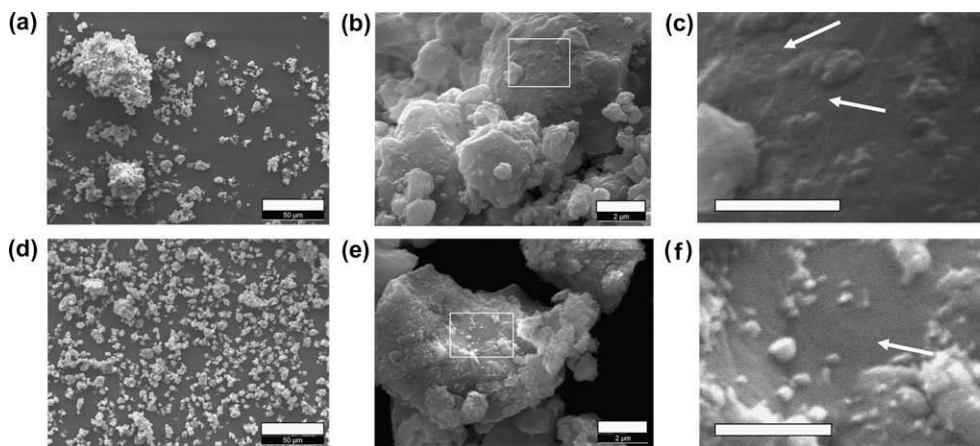


Fig. 3. Microstructure of (a–c) powder 1 and (d–f) powder 2.1 (24 h, 500 °C). Three enlargements are shown for each powder. The error bars are 50 μm (a and d), 2 μm (b and e) and 1 μm (c and f). (c) and (f) are enlargements of (b) and (e) (see frames). The arrows in (c) and (f) attempt to show the difference between powder 1 and powder 2.1: in (c) rough features are present on the surface between larger surface irregularities, whereas such features are more difficult to detect after calcination (see the arrow in (f)). Enlargement of (c) and (f): width of (c) = 3.5 μm; width of (f) = 2.5 μm.

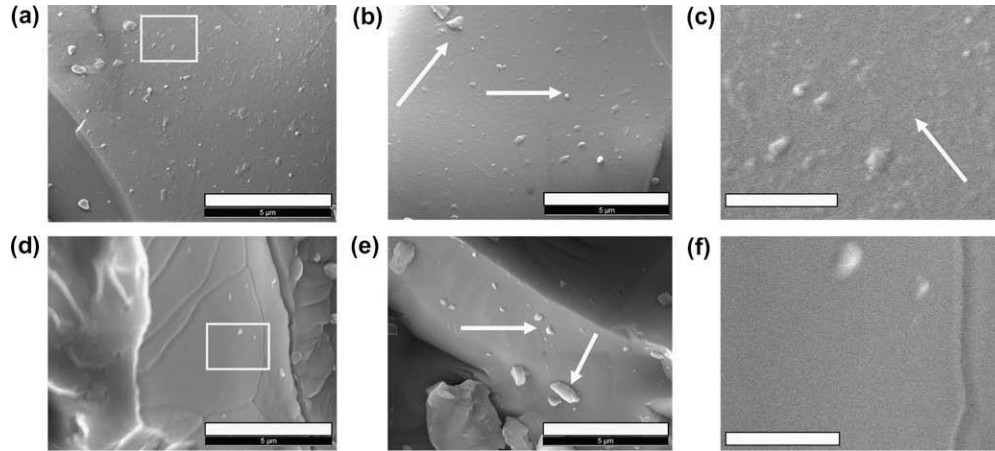


Fig. 4. Microstructure of 0.125–0.180 mm  $\alpha$ -TCP granules before (a–c) and after (d–f) a 24 h thermal treatment at 500 °C. The photos are representative of two different granules. The enlargement is the same for (a), (b), (d) and (e) (scale bars = 5  $\mu$ m). The scale bars in (c) and (f) correspond to 1  $\mu$ m. An enlarged part of (a) and (d) (see frames), respectively, is shown in (c) and (f). Before calcination, the surface is rough at the nanometer level (see the arrow in (f)), whereas after calcination no such defects can be detected. Some particles appear to be loose on the surface (see arrows).

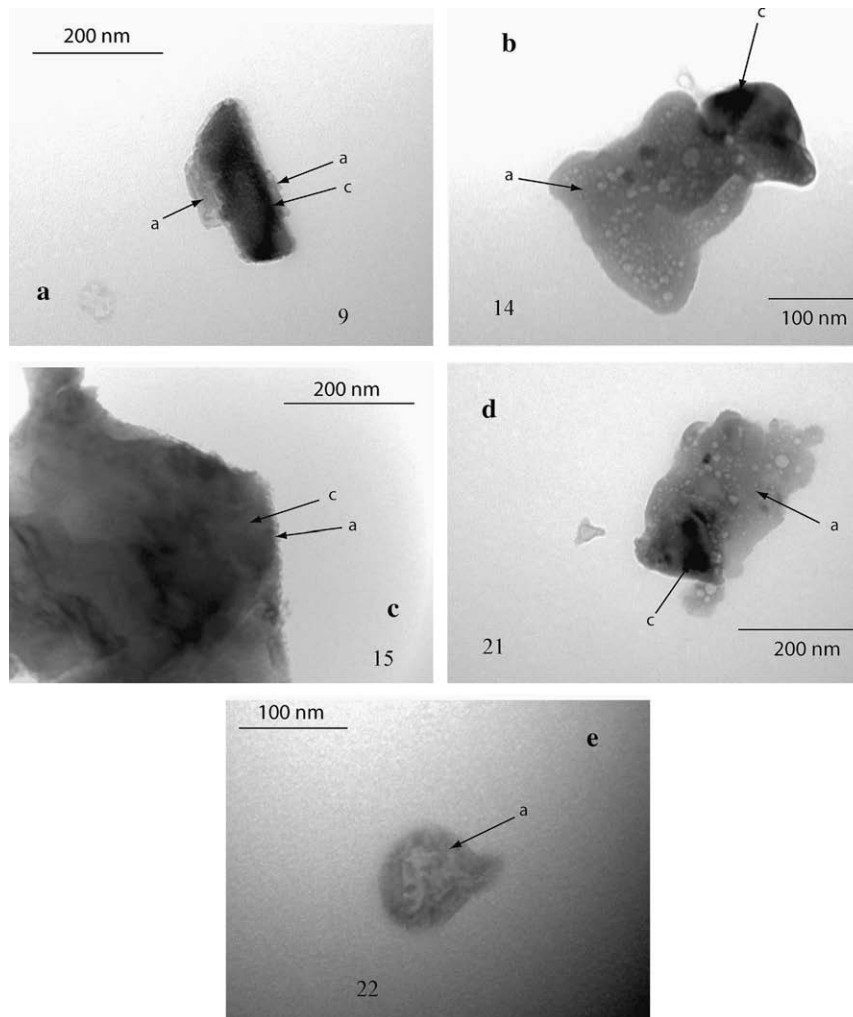


Fig. 5. Five examples of powder 1 particles surrounded by spongiform amorphous phase. In each figure, the crystalline phase of the particle is labelled “c” and the amorphous one is labelled “a”. The scale in (a), (c) and (d) is 200 nm, whereas that in (b) and (e) is 100 nm.

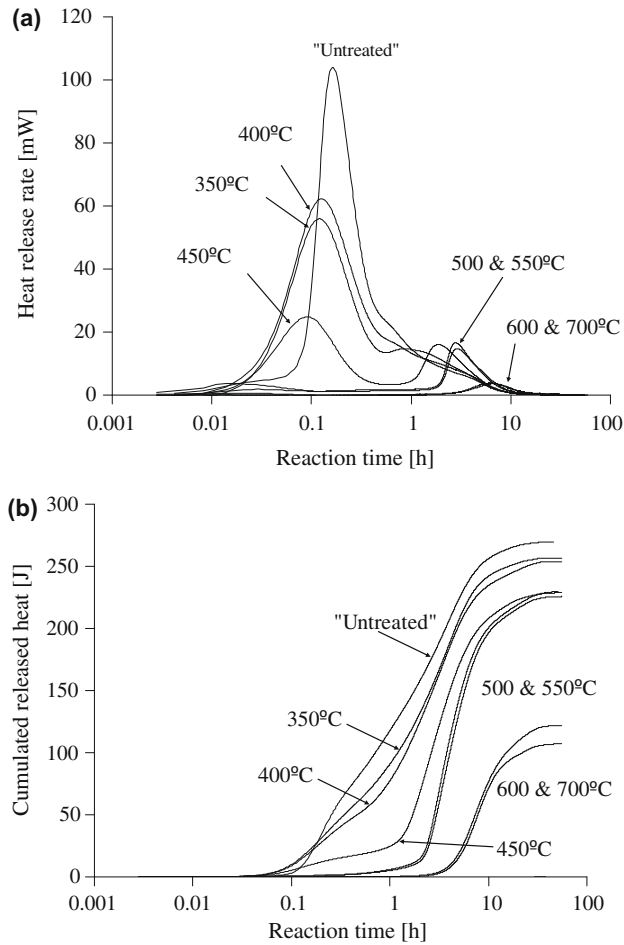


Fig. 6. Representative curves showing the effect of calcination temperature on powder reactivity. (a) Heat release rate; (b) cumulated heat release. Composition: 2 g of powder and 1 ml of 0.2 M Na<sub>2</sub>HPO<sub>4</sub> solution. The curves correspond to powders 1, 2.1 and 2.3–2.8.

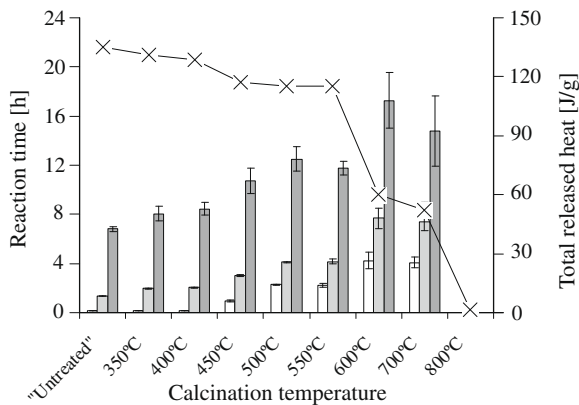


Fig. 7. Summary of the effect of the calcination temperature on (histogram bars) the time to reach a 10%, 50% and 90% released heat fraction (from left to right), and (x) the total released heat. Composition: 2 g of powder and 1 ml of 0.2 M Na<sub>2</sub>HPO<sub>4</sub> solution. Powder 1 (“untreated”) was calcined at 350 °C (powder 2.3), 400 °C (powder 2.4), 450 °C (powder 2.5), 500 °C (powder 2.1), 550 °C (powder 2.6), 600 °C (powder 2.7), 700 °C (powder 2.8) and 800 °C (powder 2.8). The error bars correspond to ±1 standard deviation. The error bars on the total released heat are too small to be seen.

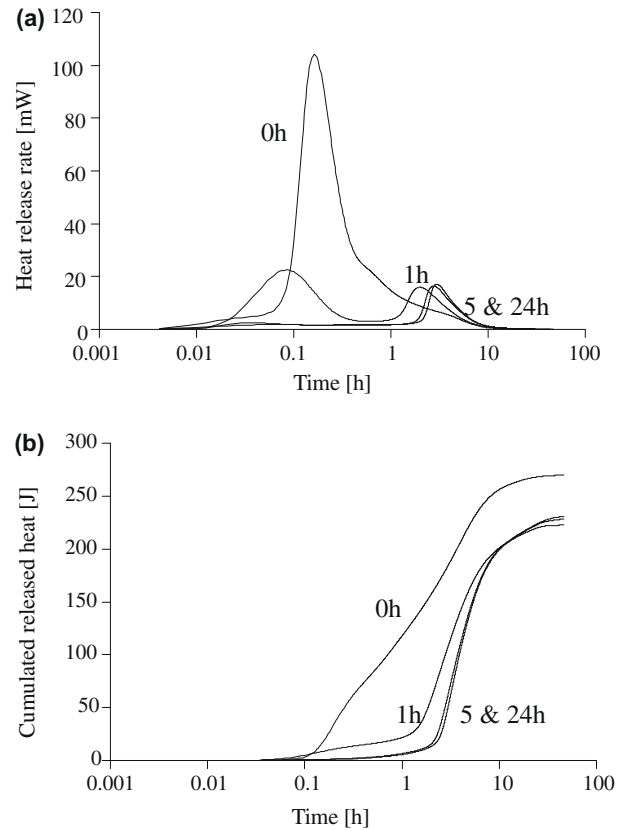


Fig. 8. Representative curves showing the effect of the calcination duration at 500 °C on the powder reactivity. (a) Heat release rate; (b) cumulated released heat. Composition: 2 g of α-TCP powder + 1 ml of 0.2 M Na<sub>2</sub>HPO<sub>4</sub> solution. Representative curves are shown here (four measurements were performed for each composition). Powder 1 (“untreated”) was calcined at 500 °C for 1 h (powder 2), 5 h (powder 2.10) and 24 h (powder 2.1).

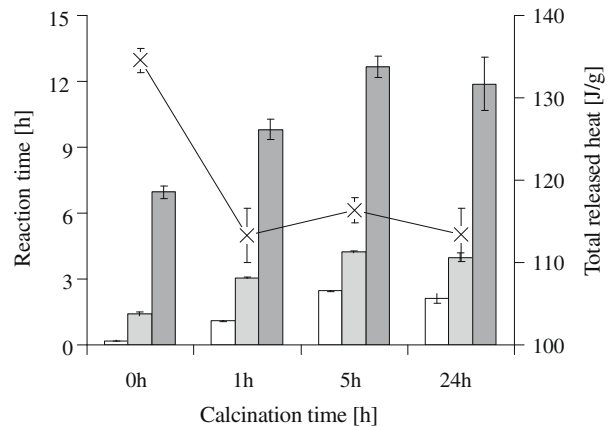


Fig. 9. Summary of the effect of the calcination duration on the powder reactivity (histogram bars) time to reach a 10%, 50% and 90% released heat fraction (from left to right); (x) total released heat. The bars correspond to the error range of the mean at  $p < 0.01$ . Composition: 2 g of α-TCP particles + 1 ml of 0.2 M Na<sub>2</sub>HPO<sub>4</sub> solution. Powder 1 (calcined, 0 h) was calcined at 500 °C for 1 h (powder 2), 5 h (powder 2.10) and 24 h (powder 2.1). The error bars correspond to ±1 standard deviation.

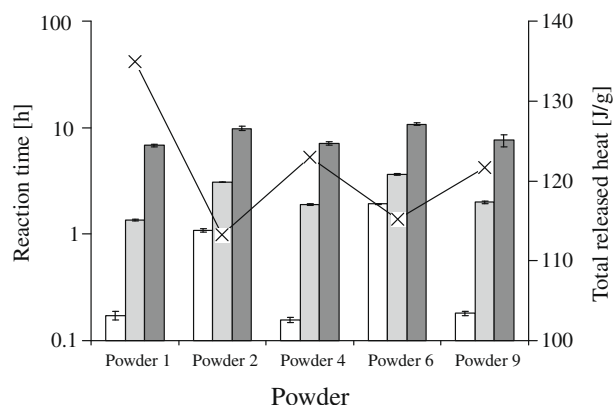


Fig. 10. Effect of calcination–milling cycles on  $\alpha$ -TCP powder reactivity (histogram bars) time to reach a 10%, 50% and 90% released heat fraction (from left to right); (x) cumulated released heat. The results of powder 1 (here shown with “–”), powder 2 (C), powder 4 (C  $\times$  M), powder 6 (C  $\times$  M  $\times$  C, calcination + milling + calcination step) and powder 9 (C  $\times$  M  $\times$  C  $\times$  M) are shown. Composition: 2 g of powder and 1 ml of 0.2 M  $\text{Na}_2\text{HPO}_4$  solution. The error bars correspond to  $\pm 1$  standard deviation.

white in the absence of calcination and after calcining the powder for 24 h at 350 °C (powder 2.3), 400 °C (powder 2.4), 600 °C (powder 2.7), 700 °C (powder 2.8) and 800 °C (powder 2.9). A slight grey colouring was observed after calcination at 450 °C (powder 2.5) and a more intense grey colouring after calcination at 500 °C and 550 °C (powder 2.6).

Four powders were analysed by XPS: (i) powder 1, (ii) powder 2.1, (iii) the precursor of the raw powder ( $\alpha$ -TCP powder not milled in the planetary milled with 0.5 ml ethanol) and (iv) the precursor of the raw powder calcined at 500 °C for 24 h. Survey XPS spectra revealed that all samples had a typical composition of tricalcium phosphates, with Ca/P molar ratios varying between 1.42 and 1.55 (Table 3). This value was increased slightly through milling (about 0.07–0.08) and reduced slightly through calcination (about 0.04–0.05). However, these changes were very limited when considering a possible change to calcium pyrophosphate (Ca/P molar ratio of 1.00). High-resolution analysis of Ca 2p, P 2p and the corresponding Auger signals and parameters did not reveal any differences between the four powders. The carbon content was low for all sam-

ples, indicating that the organic contamination was minor. The carbon content dropped by 1–2% in all calcinated samples, indicating that organic contamination was at least partially removed in the calcination step. This observation was supported by analysis of high-resolution spectra, which showed a lower organic component in the O 1s oxygen peak. High-resolution analysis of the carbon C 1s carboxylate component suggested that a thin carbonate layer was formed by calcination. Analysis of the O 1s components did not reveal additional information since the peak position of the phosphate oxygen and carbonate oxygen was very similar (0.2–0.3 eV difference).

Raman analysis of the precursor powder clearly showed the characteristic pattern of the phosphate vibrations at  $\nu_2 = 405\text{--}440\text{ cm}^{-1}$ ,  $\nu_4 = 555\text{--}630\text{ cm}^{-1}$ ,  $\nu_1 = 935\text{--}990\text{ cm}^{-1}$  and  $\nu_3 = 1025\text{--}1080\text{ cm}^{-1}$  (Fig. 11a). All spectra in Fig. 11 were measured using 782 nm excitation, a wavelength chosen to avoid fluorescence from organic residues. Calcination at 500 °C for 24 h (powder 2.1) did not change the spectra, except for the peaks at 360 and 558  $\text{cm}^{-1}$ , which are attributed to Ca–OH stretch and libration, respectively. The peak at 842  $\text{cm}^{-1}$  is due to a spike in the spectrum. Milling of the raw powders reduced signal intensity, but did not change the peak energies (Fig. 11b). The background signal was slightly more intense, however. An extremely high background signal, masking all Raman peaks of the crystalline phase, is observed for several samples after calcination of the milled powder, as illustrated in Fig. 11b. Its origin is probably not due to fluorescence, as the excitation wavelength is too long for efficient absorption. Raman spectroscopy is therefore of limited use for the characterization of calcined, milled powders.

#### 4. Discussion

The aim of the present study was to assess the effect of  $\alpha$ -TCP powder calcination on its hydraulic reactivity. The results showed that calcining  $\alpha$ -TCP powder in a temperature range of 450–550 °C did indeed affect the powder reactivity: the induction time (defined here as the time to release 10% of the total heat released during the reaction) increased by one order of magnitude, whereas the end-part of the reaction was hardly modified (Figs. 6 and 7). Importantly, this effect was observed in a temperature range in

Table 3  
Composition of  $\alpha$ -TCP powders as measured with XPS (in at.%).

Element	Sample				HA reference	Ca carbonate reference	Theoretical value for $\alpha$ -TCP
	Precursor	Calcined precursor	Powder 1	Powder 2.1			
Ca 2p	18.8	18.8	18.5	19.2	20.6	16.3	23.1
P 2p	12.6	13.2	11.9	12.7	12.2	0	15.4
O 1s	56.1	57.2	58	57.5	57.1	49.6	61.5
C 1s	12.5	10.7	11.5	10.6	10.2	34.1	–
Ca/P ratio	1.49	1.42	1.55	1.51	1.69		1.5

Four powders were analysed: (i) powder 1 (see Tables 1 and 2 for details); (ii) powder 2.1 (see Tables 1 and 2 for details); (iii) the precursor of the raw powder ( $\alpha$ -TCP powder not milled in the planetary milled; denominated “precursor”); and (iv) the precursor of the raw powder calcined at 500 °C for 24 h (denominated “calcined precursor”).

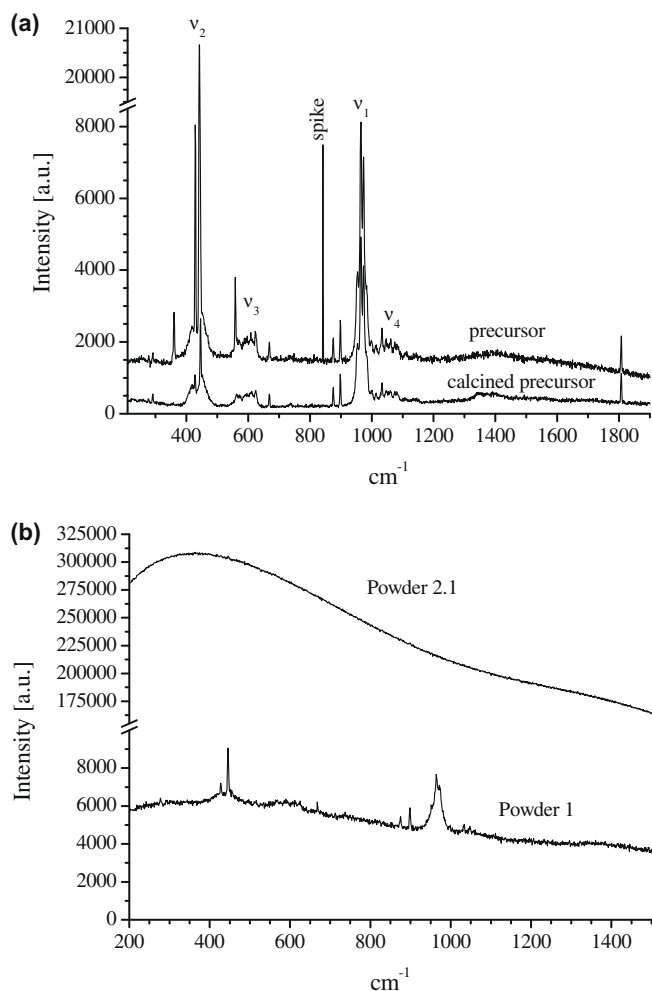


Fig. 11. Micro-Raman spectra of (i) powder 1 (denominated “raw powder”; shown in a), (ii) powder 2.1 (denominated “calcined powder”; a), (iii) the precursor of the raw powder ( $\alpha$ -TCP powder not milled in the planetary milled; denominated “precursor” in b) and (iv) the precursor of the raw powder calcined at 500 °C for 24 h (denominated “calcined precursor” in b).

which only a minor change in SSA (Table 2) was observed, with no significant changes in crystalline bulk composition, crystallite size, mean particle size or specific surface area (Figs. 1 and 2, Table 2).

Two types of reaction can be proposed to explain the data: a bulk reaction and a surface reaction. Looking first at the bulk reaction, no composition changes were observed by XRD. However, an amorphous phase was detected by TEM in the untreated powder (Fig. 5). Moreover, it is well known that XRD only detects crystalline phases and that powder milling (also called micronization [24]) transforms a crystalline powder into an amorphous powder [7,13,14]. According to Camiré et al. [7], an increase in the amorphous fraction of  $\alpha$ -TCP powder leads to an acceleration of the reaction rate and an increase in the heat released during the hydraulic reaction. In the latter study, a milling duration of 15 min (as used here) was long enough to produce noticeable changes. Looking at the cal-

orimetry results presented in this study, it appears that the untreated powder (powder 1) released more heat than the calcined powders (Fig. 6), suggesting the presence of a disordered (= amorphous) tricalcium phosphate in the untreated  $\alpha$ -TCP powder. However, even though it is likely that the presence of an amorphous fraction would accelerate the reaction, as seen by Camiré et al. [7], it is not clear how such a change could so markedly modify the initial powder reactivity (by several orders of magnitude) without similarly modifying the end-part of the reaction. The same remark can be made when looking at the reactivity of nanosized  $\alpha$ -TCP powders obtained by thermal treatment of amorphous calcium phosphate at 600–700 °C [16]: these powders, which were likely to be well crystallized throughout their bulk, were seen to barely react for the first few hours and then fully react within a few hours. A bulk explanation also appears quite unlikely when looking at millitized particles because such particles are generally obtained with very little energy (when compared to 15 mm ball milling), but still present a marked reactivity decrease due to calcination. So, the results presented in past studies [7,16] and here suggest that a surface mechanism rather than a bulk mechanism is at play. Three potential explanations involving surfaces can be proposed: the formation of an organic layer on the particle surface, the formation of an inorganic layer, and finally a physical change in the particle surface. These are discussed in the following paragraphs.

First, the effect of calcination might be explained by the presence of burnt organic residues on the particle surface after calcination, hence preventing or postponing the reaction. This assumption is based on two facts: (i) the powders were milled in the presence of small amounts of ethanol (0.5 ml in 100 g of powder); and (ii) a slight colour change was observed after calcining the powders at 450, 500 and 550 °C. To test the likelihood of this explanation, the hydraulic reactivity of  $\alpha$ -TCP granules (size between 0.125 and 1.0 mm) milled without any organic additives was determined. Calorimetry data showed that the time to reach 10% cumulated released heat was increased by 2–3 h after powder calcinations, suggesting that the effect of calcination on  $\alpha$ -TCP powder reactivity cannot be solely due to burnt organic residues. This assessment is supported by two other observations. First, the powders calcined at 600 °C (powder 2.7) also presented long induction times, even though their colour was white, suggesting an absence of organic residues on their surface. Second, Brunner et al. [17] observed a very slow hydraulic reactivity of nanosized  $\alpha$ -TCP powders obtained by calcining organic-free amorphous tricalcium phosphate powders.

The second potential explanation for the effect of calcination on reactivity is based on a chemical change in the calcium phosphate surface. For example, a phase less soluble than  $\alpha$ -TCP could form at the surface, such as  $\beta$ -TCP, oxyapatite (Ca/P molar ratio of 1.67;  $\text{Ca}_{10}(\text{PO}_4)_6\text{O}$ ) or calcium pyrophosphate (Ca/P = 1.00;  $\text{Ca}_2\text{P}_2\text{O}_7$ ; CPP). However, it appears unlikely to occur considering the results

obtained in calcination–milling cycles: even though there was always a slight but not significant increase in  $\beta$ -TCP content during each calcination step, there was no continuous change in composition during several calcination–milling cycles. This statement is also supported by TEM observations, which did not reveal the presence of a different phase at the particle surfaces, and XPS data, which revealed only minor changes in the Ca/P molar ratio at the surface (Table 3; note that before performing XPS analysis, energy-dispersive X-ray analysis was also performed but did not indicate significant changes). Furthermore, micro-Raman data revealed a change during the calcination of powder 1 (the strong signal of total symmetric  $\nu_1$  band was lost during powder 1 calcination in the strongly amplified background signal), but since no such effect was found during the calcination of the precursor powder and since the latter powder was also subjected to a change in reactivity through calcination, the change in reactivity cannot be related to the change in the micro-Raman fingerprint. The high backgrounds of powders 1 and 2.1 are likely to be due to an increased scattering of the signal at nanoparticles, or that a glass-like state-disordered phosphate layer is formed at the particle surface and disturbs the Raman excitation; however, only speculations can be made at present.

In order for a chemical (or physical) change to occur at the particle surface, it is necessary to have atomic diffusion. When a powder is submitted to a temperature close to but below its melting point, diffusion of atoms occurs, eventually leading to particle fusion [25–27]. This process is called sintering. Several sintering stages can be distinguished, ranging from neck formation and growth to substantial porosity decrease and finally pore closing. The most interesting stage for the present study is the very first reaction that occurs: particle smoothing [28]. This reaction occurs at the lowest temperature range of sintering and is not expected to affect bulk properties. However, it is expected to have a marked effect on the chemical and/or physical properties of surfaces. Here, the range of temperatures used for the thermal treatment was below the normal sintering range of calcium phosphates such as  $\alpha$ -TCP and  $\beta$ -TCP (typically above 700–800 °C) and hence could be expected to be close to or within the particle-smoothing range of  $\alpha$ -TCP and  $\beta$ -TCP. Indeed, particle smoothing was observed by SEM (Figs. 3 and 4).

The third potential explanation for the effect of calcination on the powder reactivity could be related to a physical effect. Many theories have been proposed to explain the complex dissolution kinetics of calcium phosphates and in particular apatite compounds [29]. Most of these theories speculate that chemical or physical changes occur at the particle surface. On the chemical side, Gramain et al. [30] suggested that calcium accumulation occurred during enamel dissolution, leading to a rapid decrease in dissolution rate. On the physical side, Zhang et al. [31] proposed a time reduction of the surface defects (dislocations) to explain the strong decrease in dissolution rate of dicalcium

phosphate dihydrate and octacalcium phosphate. Later, this explanation was extended by Tang et al. [18]. These authors postulated that the absence of dissolution of calcium phosphate particles in undersaturated conditions is related to the difficulty in creating surface defects, particularly on small particles. These authors introduced the concept of critical size defect in the same way as one talks about critical size nuclei in crystallization reactions. Contrary to a chemical approach, the physical approach of Tang et al. [18] implies only short-range changes at the surface. Moreover, it would provide an explanation for the reduction of total heat released during the hydraulic reaction of calcined powders (Fig. 6–10) since an increase in milling time (= increase in defect density) increases the total released heat [7]. Furthermore, it can explain the results of a recent study in which the hydraulic reactivity of nanosized  $\alpha$ -TCP powders was seen to increase with an increase in particle size [16]. Finally, it is supported by the observation that surface defects disappear during a 24 h calcination step at 500 °C.<sup>2</sup>

One might argue that these surface defects are in fact particles sticking to the surface of larger particles. A look at Fig. 4 shows that such particles are indeed present on the surfaces (arrows in Fig. 4b and e). However, it is unlikely that the roughness seen in Fig. 4c (indicated with an arrow) is made up of small single nanoparticles with a size smaller than 100 nm because planetary milling  $\alpha$ -TCP does not produce such fine powders. More specifically, the maximum specific surface area that can be reached by planetary milling is close to 3 m<sup>2</sup> g<sup>-1</sup> and the minimum mean particle diameter is limited to a few microns [7].

The effect of calcination appears to be thermodynamically driven because the effect is more potent at longer calcination times (Fig. 8) and at higher temperatures (Fig. 6). For example, the reaction curve obtained with  $\alpha$ -TCP powder calcined at 450 °C for 24 h (powder 2.5; Fig. 6) is very similar to that obtained with  $\alpha$ -TCP powder calcined at 500 °C for 1 h (powder 2; Fig. 8), suggesting that 24 h calcination duration at 450 °C is not long enough to fully “passivate” the surface. In other words, it is believed that a much longer thermal treatment at 450 °C would lead to the same passivation efficiency as 24 h at 500 °C.

Even though the use of a calcining step to modify the reactivity of calcium phosphate and more generally ceramic particles appear obvious, little can be found in the literature. In the 1970s, it was shown that laser irradiation of enamel decreased its dissolution rate in acidic conditions [32]. This effect was mostly associated with a decrease in carbonate content [33], leading to a reduction in the solubility [34–36]. Moreover, the appearance of a long induction time was not reported in most cases, or was reported only in combination with dissolution inhibitors [35]. The absence of induction time was perhaps due to the use of

<sup>2</sup> Note: this phenomenon was poorly detectable on microsized particles (powder 1 and 2.1), but was clearly detectable on large particles (Fig. 4).

low pH conditions (typically pH 4.5). In a different field, it is known that a high-temperature treatment of magnesia – the so-called “deadburned” magnesia – leads to a loss of hydraulic reactivity. To our knowledge, the mechanism has not been elucidated yet. The absence of dissolution of calcium phosphate compounds has also been reported to occur in undersaturated conditions [31], in particular with  $\beta$ -TCP [37,38]. However, the absence of dissolution was observed after a certain dissolution time, whereas here, dissolution did not occur for a certain duration (= induction time) at the start of the reaction, but then occurred readily.

The results presented in this study reveal that powder calcination can be used to control the setting rate of  $\alpha$ -TCP-based CPCs. Hitherto, such control was achieved by means of additives (e.g. HA powder, presence of ions in the mixing liquid) or by changing the particle size. Contrary to the latter two approaches, powder calcination is very potent, and is also very easy to apply. A thermal treatment at 500 °C for 5 h (powder 2.10) is long enough to achieve an extensive effect (Figs. 8 and 9). Moreover, the effect of calcination can be reversed by a short milling step (Fig. 10). Finally, the effect appears to be independent of the particle size since the delay at reacting is a few hours for nanosized- [16,17], microsized- (Fig. 6) and millisized particles (unpublished data). The potency that a calcination step has to modify the reactivity of  $\alpha$ -TCP powders should ease the optimization of the handling properties of  $\alpha$ -TCP-based CPCs.

## 5. Conclusion

Calcining a microsized  $\alpha$ -TCP powder for a few hours at 450–550 °C modified its reactivity when mixed with a 0.2 M  $\text{Na}_2\text{HPO}_4$  solution: the reaction did not start within minutes, but within hours. In other words, the effect of calcination was mostly seen to affect the start of the hydraulic reaction, even though the overall reaction was postponed. Tests made with calcination–milling cycles showed that surface passivation due to calcination could be reversed with a short milling step. Interestingly, the effect of calcination occurred in the absence of significant change in crystalline composition, crystal size, particle size and specific surface area. Also, chemical surface analysis using XPS and micro-Raman spectroscopy did not show any change in chemical composition. However, TEM results revealed the presence of an amorphous phase in the untreated powder. Moreover, physical surface analysis using SEM revealed that a calcination step of 24 h at 500 °C was able to remove small nanosized defects present at the particle surfaces. Based on the present results, four explanations were proposed and discussed: one based on a change in the bulk composition (reduction of the amorphous content) and three based on surface changes. Since the powder reactivity was mostly decreased in the early phase of the reaction, it was proposed that surface mechanisms were responsible for the observed changes. The most likely mechanism is that surface defects, which are responsible

for the initiation of particle dissolution, are removed during calcination. As a result, the creation of critical size defects, which are essential for dissolution, is slow and the whole hydraulic reaction is postponed. The possibility of markedly changing the initial hydraulic reactivity of  $\alpha$ -TCP powders via a simple calcination step opens up new perspectives in the design of better  $\alpha$ -TCP-based CPCs.

## Acknowledgements

The authors thank W. Hirsiger for SEM photos and S. Grünenfelder for her help with measuring calorimetry curves and processing some of the tested powders. Furthermore, Instrumat SA (Renens, Switzerland) is acknowledged for the PSD measurements. Finally, the reviewers are acknowledged for their pertinent comments.

## References

- [1] Bajpai PK, Fuchs CM, McCullum DE. Development of tricalcium phosphate ceramic cements. In: Lemons JE, editor. Quantitative characterization and performance of porous implants for hard tissue applications. Philadelphia, PA: ASTM; 1987. p. 377–88.
- [2] Brown WE, Chow LC. A new calcium phosphate setting cement. *J Dent Res* 1983;62:672.
- [3] Bohner M, Gbureck U, Barralet JE. Technological issues for the development of more efficient calcium phosphate bone cements: a critical assessment. *Biomaterials* 2005;26(33):6423–9.
- [4] Monma H, Goto M, Kohmura T. Effects of additives on hydration and hardening of tricalcium phosphate. *Gypsum Lime* 1984;188:11–6.
- [5] Monma H, Kanazawa T. The hydration of  $\alpha$ -tricalcium phosphate. *Yogyo-Kyokai-Shi* 1976;84(4):209–13.
- [6] Monma H, Goto M. Behavior of the a–b phase transformation in tricalcium phosphate. *Yogyo-Kyokai-Shi* 1983;91(10):473–5.
- [7] Camire CL, Gbureck U, Hirsiger W, Bohner M. Correlating crystallinity and reactivity in an alpha-tricalcium phosphate. *Biomaterials* 2005;26(16):2787–94.
- [8] Durucan C, Brown PW. Reactivity of alpha-tricalcium phosphate. *J Mater Sci* 1999;37(5):963–9.
- [9] Ginebra MP, Driessens FCM, Planell JA. Effect of the particle size on the micro and nanostructural features of a calcium phosphate cement: a kinetic analysis. *Biomaterials* 2004;25(17):3453–62.
- [10] Bohner M, Malsy AK, Camire CL, Gbureck U. Combining particle size distribution and isothermal calorimetry data to determine the reaction kinetics of  $\alpha$ -tricalcium phosphate–water mixtures. *Acta Biomater* 2006;2(3):343–8.
- [11] Bohner M. Reactivity of calcium phosphate cements. *J Mater Chem* 2007;17:3980–6.
- [12] Fernandez E, Ginebra MP, Boltong MG, Driessens FC, Ginebra J, De Maeyer EA, et al. Kinetic study of the setting reaction of a calcium phosphate bone cement. *J Biomed Mater Res* 1996;32(3):367–74.
- [13] Gbureck U, Barralet JE, Radu L, Klinger HG, Thull R. Amorphous alpha-tricalcium phosphate: preparation and aqueous setting reaction. *J Am Ceram Soc* 2004;87(6):1126–32.
- [14] Gbureck U, Grolms O, Barralet JE, Grover LM, Thull R. Mechanical activation and cement formation of beta-tricalcium phosphate. *Biomaterials* 2003;24(23):4123–31.
- [15] Baroud G, Bohner M, Heini P, Steffen T. Injection biomechanics of bone cements used in vertebroplasty. *Biomed Mater Eng* 2004;14(4):487–504.
- [16] Bohner M, Brunner TJ, Doebelin N, Tang R, Stark WJ. Effect of thermal treatments on the reactivity of nanosized tricalcium phosphate powders. *J Mater Chem* 2008;18:4460–7.

- [17] Brunner TJ, Bohner M, Grass RN, Stark WJ. Effect of particle size, crystal phase and crystallinity on the reactivity of tricalcium phosphate cements for bone reconstitution. *J Mater Chem* 2007;17:4072–8.
- [18] Tang R, Nancollas GH, Orme CA. Mechanism of dissolution of sparingly soluble electrolytes. *J Am Chem Soc* 2001;123:5437–43.
- [19] Rodriguez-Carvajal J. Recent developments of the program FULL-PROF. *Comm Powder Diffraction (IUCr) Newsl* 2001;26:12–9.
- [20] Schroeder LW, Dickens B, Brown WE. Crystallographic studies of the role of Mg as a stabilizing impurity in b-Ca<sub>3</sub>(PO<sub>4</sub>)<sub>2</sub>. II. Refinement of Mg-containing b-Ca<sub>3</sub>(PO<sub>4</sub>)<sub>2</sub>. *J Solid State Chem* 1977;22(3):253–62.
- [21] Mathew M, Schroeder LW, Dickens B, Brown WE. The crystal structure of a-Ca<sub>3</sub>(PO<sub>4</sub>)<sub>2</sub>. *Acta Cryst.* 1977;B33:1325–33.
- [22] Sudarsanan K, Young RA. Significant precision in crystal structure details: holly springs hydroxyapatite. *Acta Cryst* 1969;B25:1534–43.
- [23] Fukase Y, Eanes ED, Takagi S, Chow LC, Brown WE. Setting reactions and compressive strengths of calcium phosphate cements. *J Dent Res* 1990;69(12):1852–6.
- [24] Briggner LE, Buckton G, Bystrom K, Darcy P. The use of isothermal microcalorimetry in the study of changes in crystallinity induced during the processing of powders. *Int J Pharm* 1994;105(2):125–35.
- [25] Bannister MJ. Shape sensitivity of initial sintering equations. *J Am Ceram Soc* 1968;51(10):548–53.
- [26] Johnson DL, Cutler IB. Diffusion sintering. *J Am Ceram Soc* 1963;46(11):541–50.
- [27] Kuczynski GC. Self-diffusion in sintering of metallic particles. *AIME Trans* 1949;185:169–78.
- [28] Ring TA. *Fundamentals of ceramic powder processing and synthesis*. San Diego, CA: Academic Press; 1995.
- [29] Dorozhkin SV. A review on the dissolution models of calcium apatites. *Prog Cryst Growth Ch* 2002;44(1):45–61.
- [30] Gramain P, Thomann JM, Gumper M, Voegel JC. Dissolution kinetics of human enamel powder. I. Stirring effects and surface calcium accumulation. *J Colloid Interface Sci* 1989;128(2):370–81.
- [31] Zhang H, Nancollas GH. Dissolution deceleration of calcium phosphate crystals at constant undersaturation. *J Crystal Growth* 1992;123:59–68.
- [32] Stern RH, Sognaes RF. Laser inhibition of dental caries suggested by first tests in vivo. *J Am Dent Assoc* 1972;85(5):1087–90.
- [33] Kuroda S, Fowler BO. Compositional, structural, and phase changes in in vitro laser-irradiated human tooth enamel. *Calcif Tissue Int* 1984;36(4):361–9.
- [34] Fox JL, Yu D, Otsuka M, Higuchi WI, Wong J, Powell G. Combined effects of laser irradiation and chemical inhibitors on the dissolution of dental enamel. *Caries Res* 1992;26(5):333–9.
- [35] Fox JL, Yu D, Otsuka M, Higuchi WI, Wong J, Powell GL. Initial dissolution rate studies on dental enamel after CO<sub>2</sub> laser irradiation. *J Dent Res* 1992;71(7):1389–98.
- [36] Hsu J, Fox JL, Higuchi WI, Otsuka M, Yu D, Powell GL. Heat-treatment-induced reduction in the apparent solubility of human dental enamel. *J Dent Res* 1994;73(12):1848–53.
- [37] Bohner M, Lemaitre J, Ring TA. Kinetics of dissolution of beta-tricalcium phosphate. *J Colloid Interface Sci* 1997;190(1):37–48.
- [38] Tang RK, Wu WJ, Haas M, Nancollas GH. Kinetics of dissolution of beta-tricalcium phosphate. *Langmuir* 2001;17(11):3480–5.